

Ag(I) and Zn(II) isonicotinate complexes: Design, characterization, antimicrobial effect and CT-DNA binding studies

M. Almáši, Z. Vargová, D. Sabolová, J. Kudláčová, D. Hudecová, J. Kuchár, L. Očenášová & K. Györyová

To cite this article: M. Almáši, Z. Vargová, D. Sabolová, J. Kudláčová, D. Hudecová, J. Kuchár, L. Očenášová & K. Györyová (2015): Ag(I) and Zn(II) isonicotinate complexes: Design, characterization, antimicrobial effect and CT-DNA binding studies, Journal of Coordination Chemistry, DOI: [10.1080/00958972.2015.1101074](https://doi.org/10.1080/00958972.2015.1101074)

To link to this article: <http://dx.doi.org/10.1080/00958972.2015.1101074>

 View supplementary material 

 Accepted online: 01 Oct 2015.

 Submit your article to this journal 

 Article views: 1

 View related articles 

 View Crossmark data 

Publisher: Taylor & Francis

Journal: *Journal of Coordination Chemistry*

DOI: <http://dx.doi.org/10.1080/00958972.2015.1101074>

Ag(I) and Zn(II) isonicotinate complexes: Design, characterization, antimicrobial effect and CT–DNA binding studies

M. ALMÁŠI¹, Z. VARGOVÁ*¹, D. SABOLOVÁ², J. KUDLÁČOVÁ², D. HUDECOVÁ³, J. KUCHAR¹, L. OČENÁŠOVÁ⁴ and K. GYÖRYOVÁ¹

¹Department of Inorganic Chemistry, Faculty of Science, P. J. Šafárik University, Moyzesova 11, SK-041 54 Košice, Slovak Republic

²Department of Biochemistry, Faculty of Science, P. J. Šafárik University, Moyzesova 11, SK-041 54 Košice, Slovak Republic

³Department of Biochemistry and Microbiology, Slovak University of Technology, Radlinského 9, SK-812 37 Bratislava, Slovak Republic

⁴Department of Organic Chemistry, Faculty of Science, P. J. Šafárik University, Moyzesova 11, SK-041 54 Košice, Slovak Republic

Trinuclear Ag(I) (**1**) and dinuclear and mononuclear Zn(II) isonicotinate (**2** and **3**) complexes were prepared and characterized by X–ray crystallography, elemental analysis, IR spectroscopy and thermal analysis. Single crystal analysis of the Ag(I) complex reveals two different monodentate carboxylate coordination modes, protonated and deprotonated, respectively. IR spectra showed correlations between isonicotinate coordination modes and $\Delta(\nu_{as}-\nu_s)_{IR}$ values. In addition, the hydrogen bonds significantly influence a position of carboxylate absorption bands. Moreover, IC₅₀ and MIC data for bacteria, yeasts and filamentous fungi were determined and the binding of Ag(I) and Zn(II) complexes to calf thymus DNA was investigated using electronic absorption, fluorescence and CD measurements. Biological tests showed that the Ag(I) complex is more active than commercially used Ag(I) sulfadiazine against *E. Coli*. The fluorescence spectral results indicate that the complexes can bind to DNA through an intercalative mode. The Stern–Volmer quenching constants for investigated complexes obtained from the linear quenching plot are in the range of 1.67×10^4 to $3.42 \times 10^4 \text{ M}^{-1}$.

Keywords: Ag(I) and Zn(II) Complexes; Isonicotinate; Mid–IR spectra; Antimicrobial activity; Intercalative DNA binding; Fluorescence

*Corresponding author. Email: zuzana.vargova@upjs.sk

1. Introduction

Bacterial resistance to antibiotics and antibacterial agents continues to occur. This is not a new phenomenon, *e.g.* resistance to penicillin was documented in the 1940s by Fleming [1].

Resistance usually begins in hospital environments, where patients suffering from severe illnesses are treated with the most recent and sophisticated antibiotics.

The research presented herein provides alternatives to some of the products on the market, to widen the spectrum of microbial pathogens susceptible to silver and also to target organisms which are resistant to current silver complexes [2-6] and for other biological properties [7].

The state of knowledge about the interactions of silver metal, salts and nanoparticles with biological systems (from single-celled organisms over cell culture to whole organisms) are reviewed in Epple's and Mijnendonckx's articles [8, 9].

Development of new active metal complexes that have antibacterial [10, 11] or antimicrobial properties [12-15], enzyme inhibition activity [16] and interact with biomolecules (proteins, DNA) has been a subject of intensive investigation [17, 18].

Bioinorganic chemists focus their interest on broad-range and multifunction antibiotics. They use the combination of biologically appropriate ligand and antimicrobial metal (Zn(II), Cu(II), Ag(I)). Three ligand approaches are suggested [19-22]: *transporters*, which provide metal transport to infection, *carriers* which provide metal transport and its gradual delivery, *multifunctional ligands*, that can act as transporters, carriers and antibiotics or analgetics simultaneously.

Silver carboxylates [23, 24], amines [25], carbenes [26] and sulfoamides [27, 28] were prepared and tested to produce effective antibiotics. Results confirm that a few significant aspects influence the final antimicrobial effect: silver coordination mode, silver abundance in the molecular unit, complex stability in solution and solid state. Ag(I) pyridinecarboxylates are extensively studied as prospective antibody agents. Their structural [29-32], spectral [22, 33, 34], thermal [34], antibacterial [22, 34] and antifungal [34] properties have been described.

Zinc(II) as an essential, low toxic and bioavailable metal is also used in clinical medicine. Zinc carboxylates [35, 36, 16], amines [37, 38] and zinc complexes with Schiff-base ligands

[17, 39] with similar stable configuration of bioactive metal (like silver) are produced and studied from different points of view (structural, spectral, antimicrobial, cytotoxic, *etc.*).

Isonicotinic acid, as a part of antidepressants (nialamide, iproniazid) [40, 41], provides two donor functions (pyridine and carboxylate) for coordination. The structure of isonicotinate determines its coordination mode and application. As a spacer ligand, isonicotinate is frequently used in supramolecular architectures with unique magnetic properties [42-49]. Similar to copper isonicotinate complexes [50], silver and zinc complexes most commonly adopt coordination mode A [51-53] (scheme 1) in the solid state; modes B [54], C [55], D [56], E [57], F [58] and G [59] (scheme 1) are rare in Ag(I) and Zn(II) isonicotinates.

The flexibility of Ag(I) and Zn(II) coordination spheres allows various 2D or 3D polymeric solid-state structures with bridging isonicotinate ligands. Their low solubility provides stable composition of the complex in aqueous solution. Therefore the isonicotinate ligand with its coordination ability becomes an important driving force for broad-range and multifunction silver-based antibiotics.

To compare antimicrobial effects we prepared the polymeric Ag(I) (**1**) and Zn(II) isonicotinate complexes (**2** and **3**). Moreover, the composition and influence of their metal coordination modes and noncovalent interactions on spectral and thermal properties are discussed. Hereby we have compared the antibacterial effect of Ag(I) and Zn(II) isonicotinates (**1**, **2**, **3**) with the commercially used Ag(I) sulfadiazine. DNA-binding studies were also performed.

2. Experimental

2.1. Material and methods

Isonicotinic acid was obtained from Sigma-Aldrich and AgNO₃ from Lachema companies. The chemicals were analytically pure and used without purification. Infrared spectra of the compounds were recorded on an Avatar FT-IR 6700 spectrometer from 4000 to 400 cm⁻¹ using ATR (attenuated total reflectance) technique.

Elemental analyses were performed with a CHNOS Elemental Analyzer Vario MICRO from Elementar Analysensysteme GmbH. TG/DTG and DTA measurements were carried out using TA instruments Netsch 409 PC. The masses of prepared samples and isonicotinic acid were 15-20 mg. Samples were heated in air (flow rate 50 cm³.min⁻¹) with heating rate 9 °C.min⁻¹

from 25 to 700 °C and measured thermoanalytical curves were analyzed using the Proteus Analysis program [60].

The crystal structure of **1** was measured with Xcalibur four-circle CCD diffractometer (Oxford Diffraction) equipped with a graphite monochromator and using $Mo\ K\alpha$ radiation ($\lambda = 0.71073\ \text{\AA}$). The structure was solved by direct methods using SIR92 [61] and refined on F^2 using the SHELXL97 program [62]. All non-hydrogen atoms were refined anisotropically and hydrogens were included in the calculated positions. The isotropic thermal parameters were fixed to $1.2 U_{eq}$ of the parent atom for all hydrogens. Crystal data for **1** are listed in table 1. Figure 1 was drawn using DIAMOND software [63].

PXRD measurements of **2** and **3** were carried out at BW2 wiggler beamline of DORIS positron storage ring in DESY (Deutsches Elektronen Synchrotron, Hamburg, Germany). The patterns were collected with beam energy of 18 keV, corresponding to a wavelength of 0.68986 Å. In our experiments, we have used the gradient Si/Si (111) double crystal to monochromatize the polychromatic beam. Samples *catena*- $\{[Zn_2(INA)_4]\}_n$ (**2**) and $[Zn(INA)_2(H_2O)_4]$ (**3**) were sealed into 0.1 mm diameter quartz capillary and measured. The diffracted photons were collected using an on-site readable image plate detector OBI [64] and [65] over the 2θ range 2-20° with a step size of 0.004°. Analysis of the synchrotron powder diffraction patterns was carried out using the FullProf program package and CMPR.

1H NMR spectra were recorded in DMSO- d_6 with a Varian Mercury Plus 400 spectrometer at 400 MHz using TMS as the internal reference. Before NMR experiments, freshly prepared samples of **1**, **2** and **3** were dissolved for 3 min by ultrasonic homogenizer. After this procedure the 1H NMR experiments were performed and the samples were kept in the dark for 48 and 96 h, respectively, and the measurements were repeated.

UV-VIS measurements were also performed in DMSO with spectroscopic purity and carried out on the Analytik Jenna Specord 250 UV-VIS spectrophotometer. The concentration of solutions used in the measurements were $5\ \mu\text{mol}\cdot\text{dm}^{-3}$.

2.1.1. Preparation of *catena*- $\{[Ag_3(INA)_3(HINA)]\}_n$ (1**).** Silver nitrate (139 mg $AgNO_3$, 0.818 mmol) with isonicotinic acid (200 mg $C_5H_4N(COOH)$ (HINA), 1.620 mmol) was stirred in deionized water (15 ml). The reaction mixture was placed in a 40 ml Parr Teflon-lined stainless-steel vessel, which was heated to 90 °C with heating rate of $3\ \text{°C}\ \text{min}^{-1}$ for 72 h. Then the

reaction mixture was cooled to room temperature with cooling rate of $0.1\text{ }^{\circ}\text{C}\cdot\text{min}^{-1}$. Dry product was used for further characterization. Anal. calcd for $\text{Ag}_3\text{C}_{24}\text{H}_{16}\text{N}_4\text{O}_8$ ($M_r = 812.02$, yield: 62.7 mg, 9.4%): C, 35.45%; H, 2.09%; N, 6.89%. Found: C, 35.22%; H, 2.08%; N, 6.92%, ^1H NMR (400 MHz, $[\text{D}_6]\text{DMSO}$): δ 7.81 (d, $J = 4.63$ Hz, 1H, H_b), 8.12 (s, 0.1H, H_a), 8.75 (s, 0.9H, H_a) ppm.

2.1.2. Preparation of catena- $\{[\text{Zn}_2(\text{INA})_4]\}_n$ (2). Isonicotinic acid (50 mg, 0.406 mmol), zinc nitrate hexahydrate (120 mg, 0.404 mmol) and pyrazine (100 mg, 1.249 mmol) were dissolved in 15 cm^3 of ethanol and placed in a Parr Teflon-lined stainless-steel autoclave. The reaction mixture was heated to $125\text{ }^{\circ}\text{C}$ for 60 h with heating rate $3\text{ }^{\circ}\text{C}\cdot\text{min}^{-1}$ and finally slowly cooled at $0.15\text{ }^{\circ}\text{C}\cdot\text{min}^{-1}$ to ambient temperature. Long needle-like crystals of *catena*- $\{[\text{Zn}_2(\text{INA})_4]\}_n$ were filtered off, washed with ethanol and dried in a stream of air. Anal. calcd for $\text{C}_{24}\text{H}_{16}\text{N}_4\text{O}_8\text{Zn}_2$ ($M_r = 619.19$, yield: 68 mg, 27%): C, 46.55%; H, 2.60%; N, 9.05%. Found: C, 45.46%; H, 2.54%; N, 9.13%. ^1H NMR (400 MHz, $[\text{D}_6]\text{DMSO}$): δ 7.89 (s, 1H, H_b), 8.20 (s, 0.16H, H_a), 8.65 (s, 0.84H, H_a) ppm.

2.1.3. Preparation of $[\text{Zn}(\text{INA})_2(\text{H}_2\text{O})_4]$ (3). A mixture of isonicotinic acid (77 mg, 0.625 mmol), zinc nitrate hexahydrate (186 mg, 0.625 mmol) and pyrazine (150 mg, 1.873 mmol) was dissolved in 15 cm^3 of ethanol/water (1:1/v:v) and stored in a Parr Teflon lined-steel autoclave. The reaction mixture was heated to $110\text{ }^{\circ}\text{C}$ with heating rate $3\text{ }^{\circ}\text{C}\cdot\text{min}^{-1}$ and kept at this temperature for 100 h. The mixture was cooled to room temperature at $0.1\text{ }^{\circ}\text{C}\cdot\text{min}^{-1}$. Colorless needle-like crystals of $[\text{Zn}(\text{INA})_2(\text{H}_2\text{O})_4]$ were collected by filtration, washed with water and dried. Anal. calcd. for $\text{C}_{12}\text{H}_{16}\text{N}_2\text{O}_8\text{Zn}_1$ ($M_r = 381.65$, yield: 89 mg, 37%): C, 37.76%; H, 4.23%; N, 7.34%. Found: C, 38.16%; H, 4.52%; N, 7.78%. ^1H NMR (400 MHz, $[\text{D}_6]\text{DMSO}$): δ 7.80 (d, $J = 4.11$ Hz, 1H, H_b), 8.13 (s, 0.2H, H_a), 8.72 (s, 0.8H, H_a) ppm.

2.1.4. Biological tests

2.1.4.1. Antimicrobial activity. The antibacterial activities of Ag(I) and Zn(II) isonicotinates and free (isonicotinic acid) were evaluated by micro-dilution method using G^+ bacteria *Staphylococcus aureus* CCM 3953 and G^- bacteria *E. coli* CCM 3988 [66]. The effects of these compounds on the growth of yeasts *Candida parapsilosis* were determined by macro-dilution

method in L-shaped tubes adapted for direct measurement of absorbance [67]. Cultures of bacteria (in Mueller–Hinton growth medium) and yeasts (Sabouraud’s growth medium) were incubated under vigorous shaking. The effects of compounds on growth of filamentous fungi *Rhizopus oryzae* CCM F–8284, *Alternaria alternata* CCM F–128 and *Microsporium gypseum* CCM F–8342 were observed by macro–dilution on solidified Sabouraud’s medium during static culturing and the diameters of growing fungal colonies were measured at intervals [68, 69]. Chromatographically pure compounds were dissolved in DMSO. Its final concentration never exceeded 1.0 vol. % in either control or treated samples. Concentration of the tested compounds was 0.1×10^{-3} –2.0 mM in all experiments. The antimicrobial activity of the tested compounds was characterized by IC_{50} values (concentration of a compound which in comparison to the control inhibits the growth of model microorganisms to 50%) and also by the minimal inhibitory concentration (MIC) values (MIC of a compound which inhibits microbial growth by 100%). The IC_{50} and MIC values were read from toxicity curves. MIC experiments on subculture dishes were used to assess the minimal microbicidal concentration (MMC). Subcultures of model microorganisms were prepared separately in Petri dishes containing appropriate agar growth medium, and incubated at 30 °C for 48 h (bacteria, yeasts) and at 25 °C for 96 h (filamentous fungi). The MMC value was taken as the lowest concentration which showed no visible growth of microbial colonies on the subculture dishes.

2.1.4.2. Electronic spectral measurements. To study the binding of complexes to DNA a Varian Cary 100 UV–VIS spectrophotometer was used for absorption spectral studies. A solution of CT DNA in buffer (10 mM Tris–HCl) gave a ratio of UV absorbance at 260 and 280 nm of 1.8–1.9, indicating that the CT DNA was sufficiently free from protein. The concentration of DNA was determined using its extinction coefficient at 260 nm ($6600 \text{ mol} \cdot \text{dm}^{-3} \cdot \text{cm}^{-1}$) [70]. Concentrated stock solutions (2.5 mM) of the Ag(I) and Zn(II) complexes were prepared in DMSO. The absorption titrations in 0.01 M Tris–HCl buffer (pH = 7.4) were performed using a fixed complex concentration (25 μM) to which equivalent increments of the DNA stock solution were added to both measuring and reference cuvette, to eliminate any interference due to absorbance of nucleic acid itself.

2.1.4.3. DNA–Ethidium bromide fluorescence quenching. Fluorescence measurements were made by using a Varian Cary Eclipse spectrofluorometer. The fluorescence studies of investigated compounds with ethidium bromide (EB) have been measured to examine whether drugs are able to displace EB from its DNA–EB complex. Concentration of stock solutions was 5 mM for the Ag(I) complex and 2.5 mM for the Zn(II) complexes (because of weak solubility) in DMSO. The DNA–EB complex was prepared by adding 4 μ M EB and 20 μ M of CT DNA for measurements with **1**; 2 μ M of EB and 10 μ M of CT DNA for measurements with **2** and **3**, respectively. The fluorescence spectra of DNA–EB were measured using excitation wavelength of 510 nm, with a slit width of 10 nm for excitation and emission beams. All measurements were performed in 0.01 M Tris–HCl buffer (pH = 7.4) at 23 °C. The spectra were recorded from 560–660 nm and analyzed according to the classical Stern–Volmer equation (1) [71, 72]:

$$I_0/I = 1 + K_{SV} [Q] \quad (1)$$

where I_0 and I are the fluorescence intensities at 602 nm in the absence and presence of the quencher, respectively, K_{SV} is the Stern–Volmer quenching constant and $[Q]$ is the concentration of quencher.

2.1.4.4. CD spectroscopy. CD spectra of CT–DNA were carried out on a Jasco J–810 spectropolarimeter at room temperature with a quartz cell of 1 mm path length by concentration of CT–DNA (2.5 mM) and complex (4.5 mM). Each CD spectrum was collected after averaging over three accumulations from 230–330 nm and a scan speed of 200 nm·min⁻¹.

3. Results and discussion

3.1. Solid state studies

3.1.1. Complex 1, 2, 3 crystal structure description. Complex **1** (figure 1) crystallizes in the monoclinic space group $P2_1/c$ with two formula units in the cell. Detailed crystallographic data and processing parameters are given in table 1 and selected bond lengths and angles are noted in table 2. The two Ag(I) ions provide different coordination modes in the structure. Ag2 is coordinated by two nitrogens (N(2) and N(2)^{#2}, where #2 = $-x+1, -y+1, -z+2$) of isonicotinate ligand providing linear arrangement of ligands. Ag1 has three donors in the coordination sphere, O(1), O(3) and N(1)^{#1} (where #1 = $x-1, -y+3, z+1/2$), which form a distorted trigonal planar

Ag(I). Isonicotinate bridges Ag(1) and Ag(1)^{#3} atoms (#3 = x+1, -y+3/2, z-1/2) by monodentate carboxylate group (O(1)) and pyridine nitrogen (N(1)) and also is bonded to Ag(1) and Ag(2) by O(3) and N(2). One oxygen (O(4)) of carboxylic group is protonated. The Ag–O and Ag–N distances are typical, 2.133–2.662 and 2.135–2.278 Å, for similar Ag(I) isonicotinates [73]. In addition, [Ag(1)INA] forms 1D chains propagating along the *a* axis and [Ag(2)HINA] units connect Ag(1) ions forming 2D network. Non-covalent, π – π stacking and hydrogen bonds (see table 3) link the coordination chains into a 3D supramolecular structure. Similar building blocks were determined in isostructural complexes [74, 57], however, different links between the building units lead to different 3D networks in these structures.

Complexes **2** and **3** crystallize in the orthorhombic, chiral space group $P2_12_12_1$ with four formula units in the cell and in the triclinic space group $P\bar{1}$ with one formula unit in the cell, respectively [75, 76]. Since their single crystal analysis was already solved, we now report the powder XRD data for these two compounds. The experimental PXRD patterns correspond well with the results simulated from the single crystal data, indicating pure phases of prepared compounds (see figure S1 in the Supplementary Information). The differences in the intensities of diffraction lines can be attributed to the variation in preferred orientation of the crystallites in the powdered samples.

3.1.2. Vibrational spectroscopy. The mid-IR spectra of free HINA and its Ag(I) and Zn(II) complexes **1**, **2** and **3** were measured. The characteristic absorption bands for the complexes are given in table 4. For comparison, the table is completed by characteristic absorption bands of sodium isonicotinate and isonicotinic acid. While free HINA provides significant absorption bands at 3380 and 1697 cm^{-1} assigned to $\nu(\text{O-H})$ and $\nu(\text{C=O})$, sodium isonicotinate affords an IR spectrum with characteristic absorption bands ($\nu_{\text{as}}(\text{COO}^-)$ and $\nu_{\text{s}}(\text{COO}^-)$ at 1534 and 1410 cm^{-1}) typical for ionic carboxylate. Similar assignment was reported by Lewandowski [77] and Yuan [78].

The presence of isonicotinic acid in **1** is demonstrated by the broad absorption of $\nu(\text{O-H})$ at 3411 cm^{-1} and strong absorption of $\nu(\text{C=O})$ at 1715 cm^{-1} . Isonicotinate ligand provides two very strong absorption bands, $\nu_{\text{as}}(\text{COO}^-)$ and $\nu_{\text{s}}(\text{COO}^-)$ stretches (1543 and 1347 cm^{-1}) in **1**. Values indicate a monodentate carboxylate that was also determined from the crystal structure. The value of $\Delta\nu$ can help to assign the carboxylate coordination mode towards metal ions [79].

Expected $\Delta\nu$ values for monodentate coordination should be significantly higher than those observed for ionic compounds of the ligand and separations significantly less than ionic values are indicative of chelating and/or bridging carboxylate groups [79]. The value of $\Delta(\nu_{\text{as}}-\nu_{\text{s}})_{\text{IR}}$ is 196 cm^{-1} for **1** that indicates monodentate coordination. The value of $\Delta\nu$ for sodium isonicotinate of 124 cm^{-1} (table 4, 134 cm^{-1} was observed by Lewandowski [77]) is lower than the corresponding $\Delta\nu$ value observed in **1**. Moreover, the calculated $\Delta\nu$ values from structural data (by Nara *et al.* equation [80]) are $224, 268\text{ cm}^{-1}$ for **1**. Two calculated values correspond to two different monodentate binding modes of carboxylate, protonated and deprotonated, respectively (see figure 1). The lower experimental $\Delta\nu$ value is probably caused by weak silver–oxygen bonding (Ag(2)–O(2), 2.866 \AA) connecting the building units in the structure. Käll *et al.* described similar connection in $\text{H}[\text{Ag}(\text{NICOT})_2]$ (NICOT = nicotinate) [81].

The isonicotinate absorption bands of **2** and **3** provide similar changes toward free ligand as seen in **1**. The values of $\Delta(\nu_{\text{as}}-\nu_{\text{s}})_{\text{IR}}$ (230 cm^{-1} **2**, 262 cm^{-1} **3**) indicate monodentate carboxylate coordination in Zn(II) complexes. The calculated $\Delta\nu$ values from structural data [80] are 268 and 167 cm^{-1} . Significantly lower $\Delta\nu_{\text{calc}}$ value indicates the ionic carboxylate (in agreement with Deacon and Phillips) that also confirms the structure of **3** [76]. To explain this considerable difference, the influence of hydrogen bonds was considered. It is evident (from crystal structure) that carboxylate oxygen is connected to intermolecular hydrogen interaction that significantly influences the carboxylate vibration mode (wavenumber position of $\nu_{\text{as}}(\text{COO}^-)$ is higher, $\nu_{\text{s}}(\text{COO}^-)$ is lower than in free ligand, table 4) simulating monodentate behavior of carboxylate. The hydrogen bond effect on carboxylate vibration mode was also observed in our previous experiments with Cu(II), Zn(II) and Ag(I) pyridinecarboxylates [34, 50, 82].

3.1.3. Thermal stability. Complex **1** thermoanalytical curves (TG/DTG–DTA) are shown in figure 2. Complex **1** is thermostable to $270\text{ }^\circ\text{C}$. Thermal decomposition occurs in two steps. The first mass loss from 270 to $300\text{ }^\circ\text{C}$ with endothermic enthalpic effect (minimum at $287\text{ }^\circ\text{C}$) corresponds to isonicotinic acid release ($15.1/17.2\%$, clcd./exp.). This endothermic effect is typical for thermal behavior of isonicotinic acid and this observation was confirmed by thermogravimetric analysis of HINA (see inset of figure 2). The remaining organic part is decomposed from 300 – $600\text{ }^\circ\text{C}$ with a significant exothermic effect (maximum at $352\text{ }^\circ\text{C}$) accompanying the thermal pyrolysis. Observed mass loss (43.7%) indicates three isonicotinate

molecules released, in agreement with the calculated value 45.1%. The solid residue after thermal decomposition is silver (39.8/39.4%, clcd./exp.).

The 3D polymeric Zn(II) complex **2** and anhydrous Zn(II) complex **3** (dehydration takes place in one step from 60 to 115 °C, 4 H₂O, 18.0/18.1%, clcd./exp.) are more stable (figure 2) than the 2D polymeric Ag(I) complex **1**. They are thermostable to 410 °C and thermal decomposition processes are similar for both Zn(II) complexes above this temperature. Isonicotinate is released in a strong exothermic effect with maximum at 443 °C (**2**) and 446 °C (**3**). The experimental mass losses (73.0% **2**, 60.8% **3**) correspond with calculated ones (73.7% **2**, 60.4% **3**). The solid residue after thermal decomposition is ZnO in both cases (residual mass 26.0%/28.1% **2**, 21.6%, 22.4% clcd./exp. **3**). Similar thermal decomposition for Zn(II) isonicotinate tetrahydrate has been described [83].

Comparing thermal stability of **1** with previously studied Ag(I) complexes [34] provides evidence that covalent bond character among building blocks plays a significant role in thermal behavior. Similarly, the anhydrous Zn(II) isonicotinate higher thermal stability than anhydrous Ag(I) complexes is caused by the presence of predominantly covalent interactions in 2D or 3D directions, respectively.

3.2. Solution studies

To confirm complex composition and stability in DMSO solution UV–VIS (figure 3) and ¹H NMR (figure 4) spectra were measured.

Isonicotinic acid shows two absorptions at $\lambda_{\max} = 213$ and 260 nm on UV spectrum (figure 3). The more intense absorption belongs to $\pi^* \leftarrow \pi$ electron transfer of pyridine conjugative system and the weak signal to $\pi^* \leftarrow n$ electron transfer from lone pair presence on nitrogen.

Isonicotinic acid expresses itself by two signals H_a and H_b in the aromatic region of the ¹H NMR spectrum [84]. Assignment of the protons is shown in figure 4. Metal coordination causes the H_a signal to split and these aromatic protons change their chemical shift to lower values ($\Delta H_a = 0.64$ (**1**), 0.56 (**2**), 0.63 (**3**), compared with free acid H_a protons). Corresponding values of the chemical shifts for prepared complexes are listed in sections 2.1.1 (for **1**), 2.1.2 (**2**) and 2.1.3 (**3**), see above.

The initial UV–VIS and ^1H NMR spectra (directly after synthesis) and corresponding spectra after 48 and 96 h confirm the stability of **1**, **2** and **3** during incubation for biological testing.

3.3. Biological tests

3.3.1. Antimicrobial activity. Antimicrobial activities of free ligand and its Ag(I) and Zn(II) complexes (figure 5) by IC_{50} and MIC values are summarized in table 5.

Free HINA was antimicrobially inactive against all model bacteria G^+ *Staphylococcus aureus*, G^- *Escherichia coli*, yeasts *Candida parapsilosis* and filamentous fungi *Rhizopus oryzae*, *Alternaria alternata*, *Microsporum gypseum*. Its IC_{50} and MIC values were higher than 2 $\text{mmol}\cdot\text{dm}^{-3}$.

Growth of model microorganisms was significantly suppressed by **1**, but very weak inhibition effects were observed by **2** and **3** added in growth medium (see table 5). From the antimicrobial activities, the presence of metal ions in the prepared compounds has significant effect on biological activity in comparison to free ligand. Complex **1** inhibited the growth of G^- *E. coli* ($\text{IC}_{50} = 0.03$ mM) more compared to growth of G^+ *S. aureus* ($\text{IC}_{50} = 0.068$ mM). Total growth inhibition of *S. aureus* was observed at 0.5 $\text{mmol}\cdot\text{dm}^{-3}$ for **1** with microbicidal effect on bacterial cells; 100% growth inhibition of *E. coli* was observed even at one-fifth the concentration of 0.1 mM with microbistatistical effect on individual cells. **2** was antibacterially inactive. Growth inhibition of *S. aureus* by **3** ($\text{IC}_{50} = 0.84$ mM) was higher than the growth inhibition of G^- *E. coli* ($\text{IC}_{50} = 1.3$ mM) but its antibacterial activity was lower with comparison to **1**. Ag(I) and Zn(II) complexes significantly influenced the growth of yeasts *C. parapsilosis* (see table 5). Similar to bacteria cases, anti-yeast activity of **1** ($\text{IC}_{50} = 0.007$ mM, MIC = 0.005 mM) was higher than inhibition activity of **2** ($\text{IC}_{50} = 0.7$ mM, MIC = 1 mM) and **3** ($\text{IC}_{50} = 1.2$ mM, MIC = 2 mM), respectively. IC_{50} value of 0.007 mM for **1** indicates considerable inhibition effect.

Comparing **1** and Ag(I) isonicotinamide inhibition effect (MIC = 0.5 and 0.078 mM [85]), **1** has lower antimicrobial effect against *S. aureus*. On the other hand, 100% growth inhibition of *S. aureus* was observed at the same concentration (MIC = 0.5 mM) in the case of Zn(II) 4-hydroxybenzoate [86]. In contrary, antibacterial effect of **2** and **3** was lower ($\text{IC}_{50} > 2$ mM, $\text{IC}_{50} = 1.3$ mM).

While **1** showed antifungal activity, **2** and **3** were inactive against filamentous fungi (IC_{50} , MIC > 2 mM). Based on a comparison of IC_{50} values (table 5) it can be concluded that inhibition fungal growth in the presence of **1** decreases in the following order: *R. oryzae* > *A. alternata* > *M. gypseum*.

Total growth inhibition of *A. alternata* and *M. gypseus* by Ag(I) complex was the same (MIC = 1 mmol·dm⁻³), however with different effect on fungal spores, microbicidal effect for *A. alternata* and microbistatistical effect for *M. gypseus*, respectively.

Complex **1** offers higher antibacterial effect than [Ag(INA)₂].4H₂O [22] against G⁻ bacteria *E. coli*. Moreover, its antibacterial effect (against *E. coli*) was more than two times higher (IC_{50} = 0.03 mM) than commercially used polymeric Ag(I) sulfadiazine (IC_{50} = 0.073 mM) [87].

Ag(I) and Zn(II) nitrates were tested toward the microorganisms (table 5). It is evident that nitrates show higher antimicrobial activity than **1**, **2** and **3**. Moreover, the antimicrobial effect of the Ag(I) isonicotinate (**1**) is considerably lower than in the case of pyridinecarboxylate analogues ([AgPIC], [AgNIC], [Ag(HDIPIC)].0.75 H₂O [29]). The results correspond with Abarca's idea that increasing antimicrobial activity of Ag(I) complexes is influenced by ligand–biological fragment exchange reactions, silver composition (63 wt. % Ag in AgNO₃, 40 wt. % in **1**, 30 wt. % Ag(I) sulfadiazine) and silver coordination mode (AgNO₃ – predominantly ionic interactions, **1** – predominantly covalent interactions) [22].

3.3.2. Electronic absorption spectra. Electronic absorption spectra are initially employed to determine the binding of complexes to DNA. Intercalation of the chromophore into the double helix usually results in hypochromism. The former phenomenon can be ascribed to decrease of the $\pi \rightarrow \pi^*$ transition energy as π^* orbital of the intercalated compound couples with the π orbital of the base pairs [88, 89].

The absorption spectrum of the Ag(I) complex consists of two well–resolved bands with maxima at 213 and 267 nm. Upon addition of CT–DNA the absorption at 267 nm showed significant hypochromic effect (about 50%) and slight red shift of this maximum about 2 nm (figure 6). These phenomena indicate that the complex interacts with CT–DNA by intercalation [72]. Similar spectroscopic behavior was observed for **2** and **3**. The binding parameters from spectrophotometric analysis are summarized in table 6.

3.3.3. Fluorescence spectral studies. Intercalative binding is also demonstrated through quenching experiments using ethidium bromide (EB). The fluorescence intensity of EB in the presence of DNA can be greatly enhanced due to intercalation with DNA [90]. On addition of **1-3** to a DNA–EB mixture, the metal complex competes with EB to bind with DNA [91]. This leads to decrease in the binding sites of DNA available for EB, and hence quenching of fluorescence intensity of the DNA–EB mixture occurs (figure 7A, B, C). The quenching plot illustrates that the quenching of EB bound to DNA by metal complexes is in agreement with the linear Stern–Volmer equation [92].

The determined Stern–Volmer constants decreased in the order ($3.42 \times 10^4 \text{ M}^{-1}$) for **1** < ($2.19 \times 10^4 \text{ M}^{-1}$) for **2** < ($1.67 \times 10^4 \text{ M}^{-1}$) for **3**. It was established that the K_{SV} value of Ag(I) complex is approximately two–times higher than the K_{SV} value of **3**. The determined K_{SV} values are close to the constants obtained for other zinc complex by Anjomshoa *et al.* [93]. These measurements show that the interactions of **1-3** with DNA are strong, probably due to intercalative binding [72, 92].

3.3.4. Circular dichroic spectral studies. Circular dichroism (CD) spectroscopy is an optical technique measuring a difference in the absorption of left and right circularly polarized light. CD experiment was performed to define the orientation of the compounds with respect to the DNA helix. The compounds have no circular dichroism spectra when free in solution but have an induced CD spectrum when in the complex with DNA. The *B*–form conformation of DNA shows two CD bands in the UV region, a positive band at 278 nm due to the base stacking and a negative band at 246 nm due to the polynucleotide helicity [94, 95]. When Ag(I) complex was incubated with CT–DNA, the positive band showed an increase in molar ellipticity and the negative band showed a decrease in intensity at 246 nm with a slight red shift of the band maximum (figure 8). Similar spectra are found for the Zn(II) complexes. The helical band at 246 nm corresponds to DNA unwound extent exhibiting decrease for all the compounds in similar order as that of previously studied Cu complexes [89]. However, the observed CD spectral changes are typical for intercalative binding [96].

4. Conclusion

The synthesis of Ag(I) and Zn(II) isonicotinate complexes has been accomplished and their structural, spectral, thermal and antimicrobial properties were described, correlated and compared. Ag(I) structural polymorph shows a new 3D structure in solid state and highest antimicrobial effect in comparison to its Zn(II) analogues.

The interaction of the synthesized complexes with CT–DNA has been performed with UV spectroscopy revealing their ability to bind to DNA. Competitive binding experiments show that the enhanced emission intensity of ethidium bromide in the presence of DNA was quenched by addition of Ag(I) and Zn(II) complexes, indicating that they displace EB from its binding site in DNA. From UV–VIS and fluorescence studies the complexes can bind to CT–DNA by intercalation. CD measurements confirm the mentioned mode of binding, which correlates well with aromatic ring system in the ligand. *In vitro* antimicrobial screening showed that Ag(I) complex was most active against tested yeasts *C. parapsilosis* with an IC₅₀ value of 0.007 mM and two times more active against bacteria *E. Coli* than similar polymeric complex Ag(I) sulfadiazine, commercially used.

Acknowledgements

This work was supported by the Slovak Research and Development Agency under contract No. APVV–0280–11, by VEGA 1/0001/13, VEGA 1/0535/16 and VVGS PF–2015–488. The authors are very grateful to Mária Vojtasová and Prof. Ján Imrich from NMR Laboratories, Department of Organic Chemistry, P. J. Šafárik University in Košice for the NMR spectra measurements.

References

- [1] A. Fleming, *New York Times*, 26 June 1945: 21.
- [2] R.J. Curran, Silver(I) Complexes as Antimicrobial and Anticancer Drugs, *Thesis presented for the Ph.D. degree*, The National University of Ireland National University of Ireland Maynooth (2009).
- [3] M.A. Iqbal, R.A. Haque, S.F. Nasri, A.M.S.A. Majid, M.B.K. Ahamed, E. Farsi, T. Fatima. *Chem. Cent. J.*, **7**, 27 (2013).
- [4] M.J. Panzner. *Dalton Trans.*, **35**, 7308 (2009).
- [5] R.R. Butorac. *Molecules*, **16**, 2285 (2011).

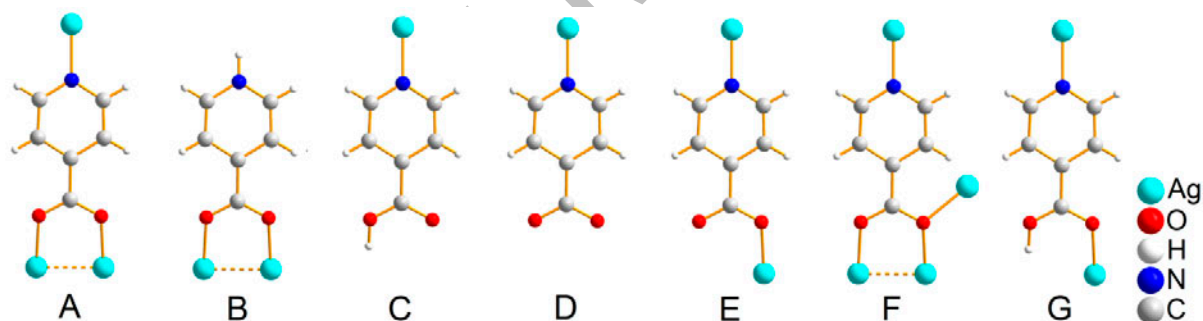
- [6] S. Pal. *J. Antimicrob. Chemother.*, **10**, 2134 (2010).
- [7] R. Behra, L. Sigg, M.J.D. Clift, F. Herzog, M. Minghetti, B. Johnston, A. Petri–Fink, B. Rothen–Rutishauser. *J. Royal Soc. Interface*, **10**, 87 (2013).
- [8] S. Chernousova, M. Epple. *Angew. Chem. Int. Ed.*, **52**, 1636 (2013).
- [9] K. Mijndonckx, N. Leys, J. Mahillon, S. Silver, R.V. Houdt. *Biometals*, **26**, 609 (2013).
- [10] H.K. Syed, M.A. Iqbal, R.A. Haque, K.K. Peh. *J. Coord. Chem.*, **68**, 1088 (2015).
- [11] R.A. Haque, P.O. Asekunowo, M.R. Razali. *J. Coord. Chem.*, **67**, 2131 (2014).
- [12] S.M. Jadhav, V.A. Shelke, S.G. Shankarwar, A.S. Munde, T.K. Chondhekar. *J. Saudi Chem. Soc.*, **18**, 27 (2014).
- [13] J. Devi, N. Batra. *Spectrochim. Acta, Part A*, **135**, 710 (2015).
- [14] P.O. Asekunowo, R.A. Haque. *J. Coord. Chem.*, **67**, 3649 (2014).
- [15] S.M. Tailor, U.H. Patel. *J. Coord. Chem.*, **68**, 2192 (2015).
- [16] N. Ali, M.N. Tahir, S. Ali, M. Iqbal, K.S. Munawar, S. Perveen. *J. Coord. Chem.*, **67**, 1290 (2014).
- [17] M. Li, Y. Gou, Y. Zhang, F. Yang, H. Liang. *J. Coord. Chem.*, **67**, 929 (2014).
- [18] H. Wu, Y. Zhang, H. Wang, Y. Bai, F. Shi, X. Wang, Z. Yang. *J. Coord. Chem.*, **67**, 1771 (2014).
- [19] M.A. Phaniband, S.D. Dhumwad, S.R. Pattan. *Med. Chem. Res.*, **20**, 493 (2011).
- [20] M. Kalanithi, M. Rajarajan, P. Tharmaraj, S.J. Raja. *Med. Chem. Res.*, **24**, 1578 (2015).
- [21] C. Núñez, A. FernándezLodeiro, J. Fernández–Lodeiro, J. Carballo, J.L. Capelo, C. Lodeiro. *Inorg. Chem. Commun.*, **45**, 61 (2014).
- [22] R. Abarca, G. Gomez, C. Velasquez, M.A. Paez, M. Gulppi, A. Arrieta, M.I. Azocar. *Chin. J. Chem.*, **30**, 1631 (2012).
- [23] X.Y. Lu, J.W. Ye, D.K. Zhang, R.X. Xie, R.F. Bogale, Y. Sun, L.M. Zhao, Q. Zhao, G.L. Ning. *J. Inorg. Biochem.*, **138**, 114 (2014).
- [24] C.N. Banti, A.D. Giannoulis, N. Kourkoumelis, A.M. Owczarzak, M. Kubicki, S.K. Hadjikakou. *J. Inorg. Biochem.*, **142**, 132 (2015).
- [25] R. Kumar, S. Obrai, A. Kaur, M.S. Hundal, H. Meehnian, A.K. Jana. *New J. Chem.*, **38**, 1186 (2014).

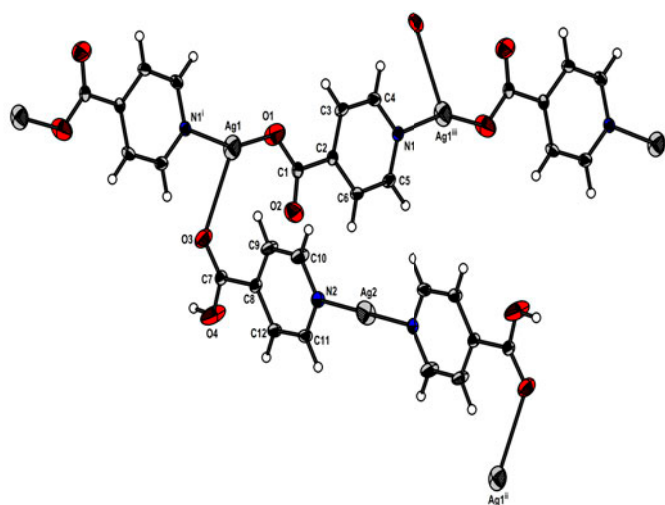
- [26] R.A. Haque, S.Y. Choo, S. Budagumpi, M.A. Iqbal, A.A. Al Ashraf. *Eur. J. Med. Chem.*, **90**, 82 (2015).
- [27] H.J. Klasen. *BURNS*, **26**, 131 (2000).
- [28] J.H.B. Nunes, R.E.F. de Paiva, A. Cuin, W.R. Lustrri, P.P. Corbi. *Polyhedron*, **85**, 437 (2015).
- [29] J.P. Deloume, R. Faure, H. Loiseleur. *Acta Crystallogr., Sect. B: Struct. Sci.*, **33**, 2709 (1977).
- [30] P.O. Käll, J. Grins, M. Fahlman, F. Söderlind. *Polyhedron*, **20**, 2747 (2001).
- [31] G. Smith, A.N. Reddy, K.A. Byriel, C.H.L. Kennard. *Polyhedron*, **13**, 2425 (1994).
- [32] M.G.B. Drew, R.W. Matthews, R.A. Walton. *J. Chem. Soc. A*, 1405 (1970).
- [33] M. Kalinowska, M. Borawska, R. Świsłocka, J. Piekut, W. Lewandowski. *J. Mol. Struct.*, **419**, 834 (2007).
- [34] Z. Vargová, M. Almáši, D. Hudecová, D. Titková, I. Rostášová, V. Zeleňák, K. Györyová. *J. Coord. Chem.*, **67**, 1002 (2014).
- [35] V.M. Manikandamathavan, T. Weyhermuller, R.P. Parameswari, M. Sathishkumar, V. Subramanian, B.U. Nair. *Dalton Trans.*, **43**, 13018 (2014).
- [36] M. Kalinowska, L. Mazur, J. Piekut, Z. Rzaczyńska, B. Laderiere, W. Lewandowski. *J. Coord. Chem.*, **66**, 334 (2013).
- [37] A. Zamani, M. Salehi, S.M. Sajjadi, M. Kubicki, G. Dutkiewicz, A. Khaleghian. *J. Coord. Chem.*, **67**, 1782 (2014).
- [38] H. López-Sandoval, M.E. Londoño-Lemos, R. Garza-Velasco, I. Poblano-Meléndez, P. Granada-Macías, I. Gracia-Mora, N. Barba-Behrens. *J. Inorg. Biochem.*, **102**, 1267 (2008).
- [39] O.A. El-Gammal, G.M.A. El-Reash, T.A. Yousef, M. Mefreh. *Spectrochim. Acta, Part A*, **146**, 163 (2015).
- [40] W. Andrew, *Pharmaceutical Manufacturing Encyclopedia*, third edn., Elsevier (2006).
- [41] R.A. Maxwell, S.B. Eckhardt, *Drug Discovery*, Humana Press (1990).
- [42] Y.H. Liu, Y.L. Lu, H.L. Tsai, J.C. Wang, K.L. Lu. *J. Solid State Chem.*, **158**, 315 (2001).
- [43] B.P. Yang, H.Y. Zeng, Z.C. Dong, J.G. Mao. *J. Coord. Chem.*, **56**, 1513 (2003).
- [44] Y. Fan, B. Li. *Inorg. Chem. Commun.*, **22**, 37 (2012).
- [45] J. Li, Y.G. Chen, C.J. Zhang, Q.J. Kong. *J. Mol. Struct.*, **921**, 233 (2009).

- [46] J. Zhang, Y. Kang, J. Zhang, Z.J. Li, Y.Y. Qin, Y.G. Yao. *Eur. J. Inorg. Chem.*, 2253 (2006).
- [47] Y. Li, F.K. Zheng, J.P. Zou, W.Q. Zou, H.W. Ma, G.C. Guo, C.Z. Lu, J.S. Huang. *Inorg. Chem. Commun.*, **10**, 787 (2007).
- [48] C.M. Wang, Y.L. Chuang, S.T. Chuang, K.H. Lii. *J. Solid State Chem.*, **177**, 2305 (2004).
- [49] F.P. Liang, M.L. Huang, C.F. Jiang, Y. Li, R.X. Hu. *J. Coord. Chem.*, **60**, 2343 (2007).
- [50] M. Almáši, Z. Vargová, R. Gyepes, R. Varga, V. Zeleňák. *Inorg. Chem. Commun.*, **46**, 118 (2014).
- [51] Z.Q. Yan. *Chin. J. Struct. Chem.*, **24**, 315 (2005).
- [52] B. Liu, Q. Yuan. *Inorg. Chem. Commun.*, **8**, 1022 (2005).
- [53] Z. Liu, P. Liu, Y. Chen, J. Wang, M. Huang. *New J. Chem.*, **29**, 474 (2005).
- [54] Q. Yuan, B. Liu. *Bull. Korean Chem. Soc.*, **26**, 1575 (2005).
- [55] B. Li, P. Gao, L. Ye, G.D. Yang, L.X. Wu. *Acta Crystallogr., Sect. E: Struct. Rep. Online*, **62**, m3238 (2006).
- [56] F. Jaber, F. Charbonnier, R. Faure, M. Petit-Ramel. *Z. Kristallogr.*, **209**, 536 (1994).
- [57] B. Cova, A. Briceno, R. Atencio. *New J. Chem.*, **25**, 1516 (2001).
- [58] W.G. Lu, J.Z. Gu, L. Jiang, C.Y. Su, T.B. Lu. *Chin. J. Inorg. Chem.*, **22**, 1977 (2006).
- [59] F.T. Xie, H.Y. Bie, L.M. Duan, G.H. Li, X. Zhang, J.Q. Xu. *J. Solid State Chem.*, **178**, 2858 (2005).
- [60] Proteus Analysis (5.2.1), NETZSCH Gerätebau GmbH, Bayern, Germany.
- [61] A. Altomare, G. Cascarano, C. Giacovazzo, A. Guagliardi. *J. Appl. Crystallogr.*, **26**, 343 (1993).
- [62] G.M. Sheldrick, SHELXL-97, Program for the Refinement of Crystal Structures, 394 University of Göttingen, Göttingen (1997).
- [63] K. Brandenburg, DIAMOND, Version 2.1e, Crystal Impact GbR, Bonn (2000).
- [64] M. Knapp, V. Joco, C. Baetz, H.H. Brecht, A. Berghaeuser, H. Ehrenberg, H. von Seggern, H. Fuess. *Nucl. Instrum. Methods A*, **521**, 565 (2004).
- [65] M. Knapp, C. Baetz, H. Ehrenberg, H. Fuess. *J. Synchrotron. Rad.*, **11**, 328 (2004).
- [66] S. Jantová, D. Hudecová, Š. Stankovský, K. Špírková, Ľ. Ružeková. *Folia Microbiol.*, **40**, 611 (1995).

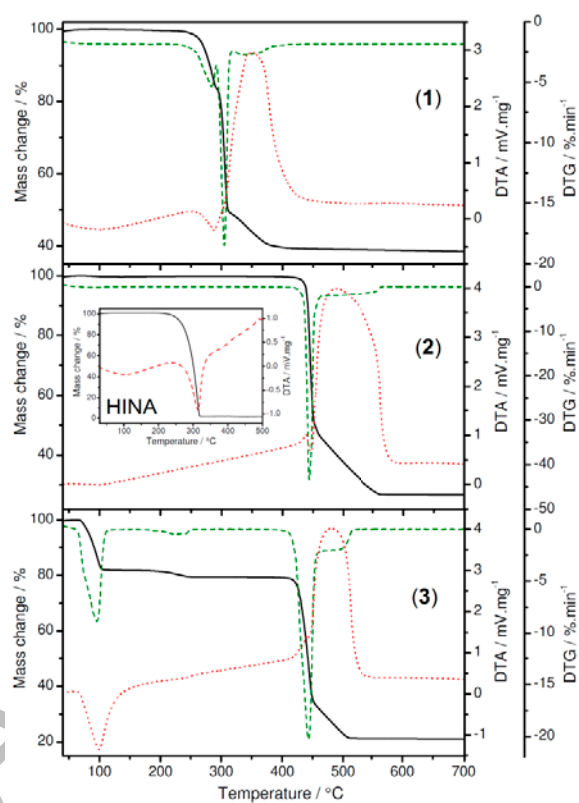
- [67] V. Betina, D. Mičková. *Z. Allg. Microbiol.*, **5**, 355 (1972).
- [68] D. Hudecová, S. Jantová, M. Melník, M. Uher. *Folia Microbiol.*, **40**, 473 (1996).
- [69] B. Dudová, D. Hudecová, R. Pokorný, M. Mičková, M. Palicová, P. Segl'a, M. Melník. *Folia Microbiol.*, **47**, 225 (2002).
- [70] M. Sirajuddin. *J. Photochem. Photobiol., B*, **124**, 1 (2013).
- [71] J.R. Lakowicz, G. Weber. *Biochemistry*, **12**, 4161 (1973).
- [72] P. Vranec, I. Potočník, D. Sabolová, V. Farkasová, Z. Ipóthová, J. Pisarčíková, H. Paulíková. *J. Inorg. Biochem.*, **131**, 37 (2014).
- [73] <http://www.ccdc.cam.ac.uk>
- [74] F.T. Xie, H.Y. Bie, L.M. Duan, G.H. Li, X. Zhang, J.Q. Xu. *J. Solid State Chem.*, **178**, 2858 (2005).
- [75] O.R. Evans, R.G. Xiong, Z. Wang, G.K. Wong, W. Lin. *Angew. Chem. Int. Ed.*, **38**, 536 (1999).
- [76] P.S. Zhao, F.F. Jian, C.L. Li. *Polish J. Chem.*, **79**, 1041 (2005).
- [77] P. Koczoń, J. Piekut, M. Borawska, W. Lewandowski. *J. Mol. Struct.*, **651–653**, 651 (2003).
- [78] B. Liu, Q. Yuan. *Inorg. Chem. Commun.*, **8**, 1022 (2005).
- [79] G.B. Deacon, R.J. Phillips. *Coord. Chem. Rev.*, **33**, 227 (1980).
- [80] M. Nara, H. Torii, M. Tasumi. *J. Phys. Chem.*, **100**, 19812 (1996).
- [81] P.O. Käll, J. Grins, M. Fahlman, F. Söderlind. *Polyhedron*, **20**, 2747 (2001).
- [82] Z. Vargová, V. Zeleňák, I. Císařová, K. Györyová. *Thermochim. Acta*, **423**, 149 (2004).
- [83] M. Chakraborty, J.N. Ganguli, S.J. Bora, B.K. Das. *Indian J. Chem.*, **49A**, 876 (2010).
- [84] http://sdbs.riondb.aist.go.jp/sdbs/cgi-bin/direct_frame_top.cgi
- [85] M.A.M. Abu-Youssef, R. Dey, Y. Gohar, A.A. Massoud, L. Öhrström, V. Langer. *Inorg. Chem.*, **46**, 5893 (2007).
- [86] K. Homzová, K. Györyová, Z. Bujdošová, D. Hudecová, M. Ganajová, Z. Vargová, J. Kovářová. *J. Therm. Anal. Calorim.*, **116**, 77 (2014).
- [87] M. McCann, R. Curran, M. Ben-Shoshan, V. McKee, M. Devereux, K. Kavanagh, A. Kellett. *Polyhedron*, **56**, 180 (2013).
- [88] T.C. Jenkins, K.R. Fox (Eds.), *Methods in Molecular Biology*, Humana Press, Totowa, New Jersey (1997).

- [89] D. Sabolová, M. Kožurková, T. Plichta, Z. Ondrušová, D. Hudecová, M. Šimkovič, H. Paulíková, A. Valent. *Int. J. Biol. Macromol.*, **48**, 319 (2011).
- [90] R.R. Pulimamidi, R. Nomula, R. Pallepogu, H. Shaik. *Eur. J. Med. Chem.*, **79**, 117 (2014).
- [91] W. Chu, Y. Wang, S. Liu, X. Yang, S. Wang, S. Li, G. Zhou, X. Qin, C. Zhou, J. Zhang. *Bioorg. Med. Chem. Lett.*, **23**, 5187 (2013).
- [92] M. Sirajuddin, S. Ali, A. Badshah. *J. Photochem. Photobiol., B*, **124**, 1 (2013).
- [93] M. Anjomshoa, H. Habadzadeh, S.J. Fatemi, M. Torkzadeh–Mahani. *Spectrochim. Acta, Part A*, **127**, 511 (2014).
- [94] M. Kožurková, D. Sabolová, L. Janovec, J. Mikeš, J. Kovaľ, J. Ungvarský, M. Štefanišínová, P. Fedoročko, P. Kristián, J. Imrich. *Bioorg. Med. Chem.*, **16**, 3976 (2008).
- [95] W. Li, Y.Y. Ji, J.W. Wang, Y.M. Zhu. *DNA Cell Biol.*, **31**, 1046 (2012).
- [96] V. Uma, M. Kanthimathi, T. Weyhermuller, B.U. Nair. *J. Inorg. Biochem.*, **99**, 2299 (2005).

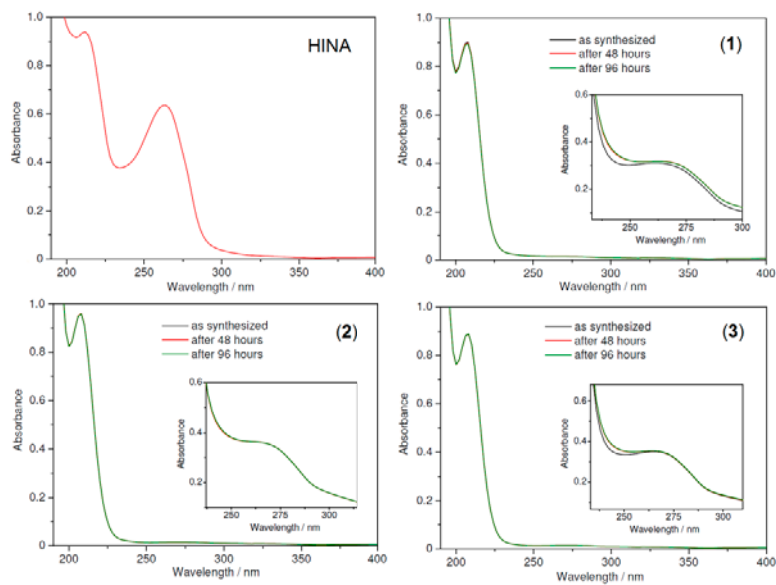




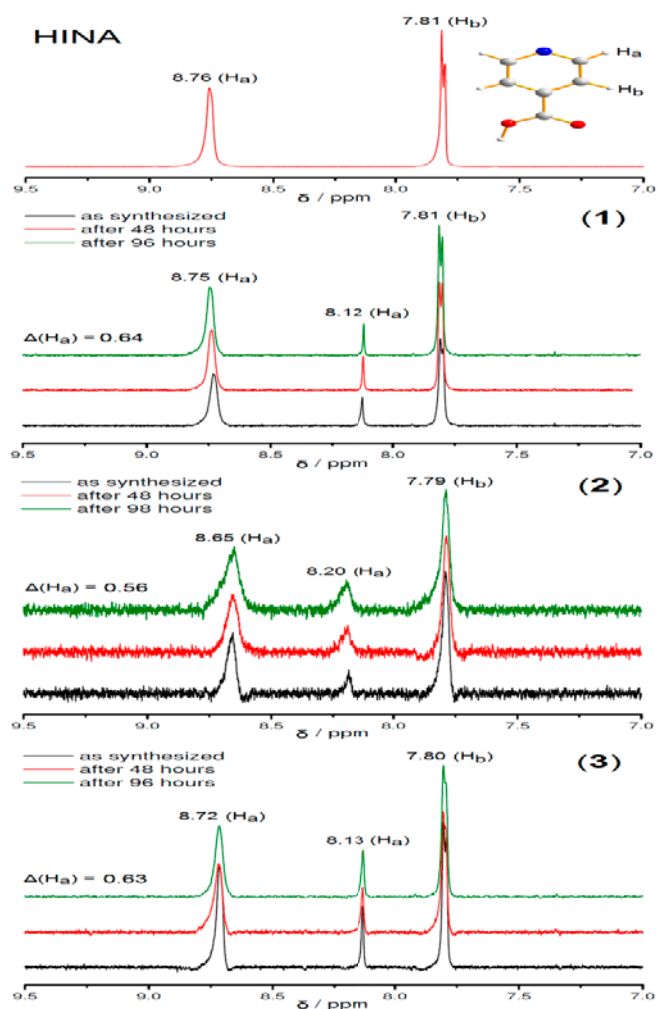
i: $x-1, -y+3/2, z+1/2$ ii: $-x+1, -y+1, -z+2$ iii: $x+1, -y+3/2, z-1/2$



A

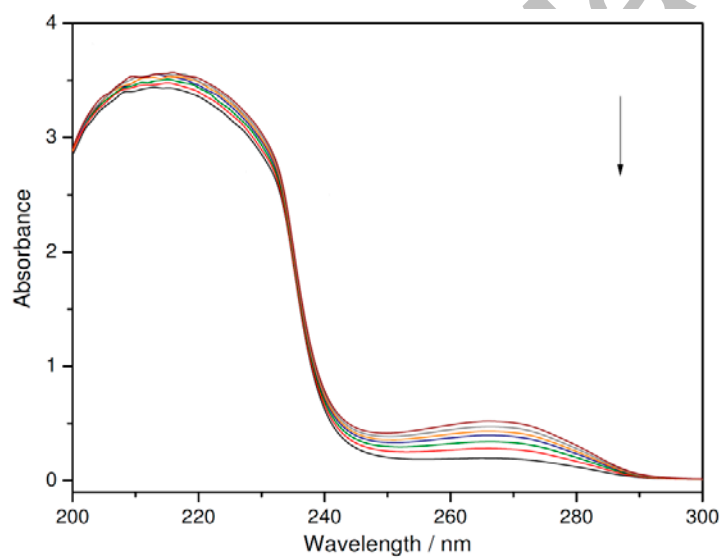
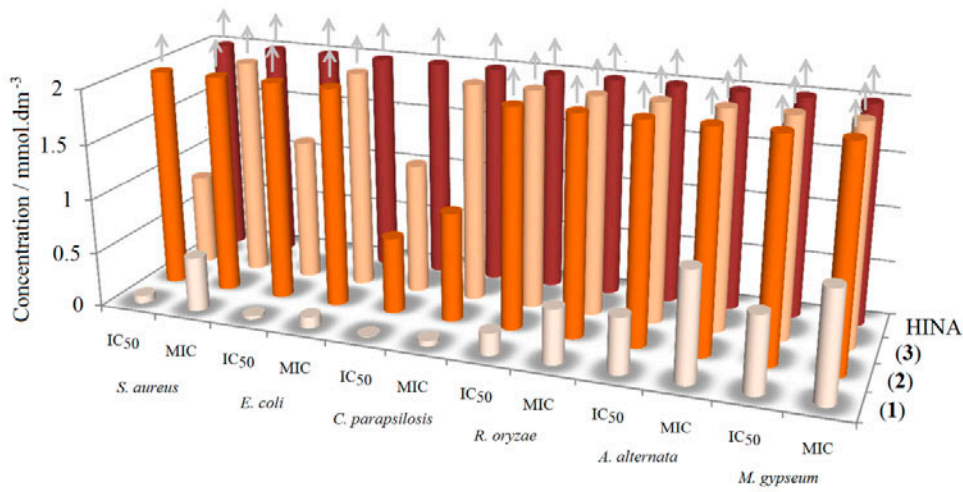


Accepted Manuscript

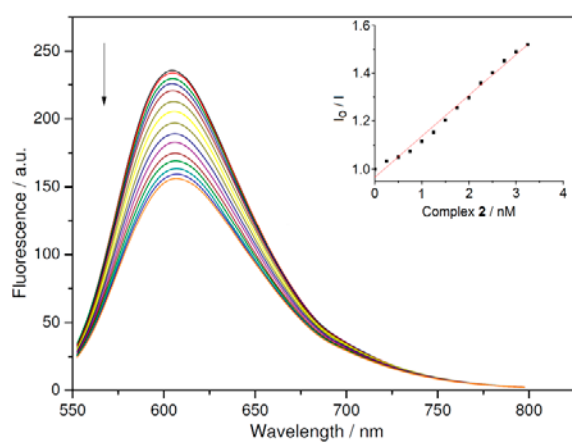
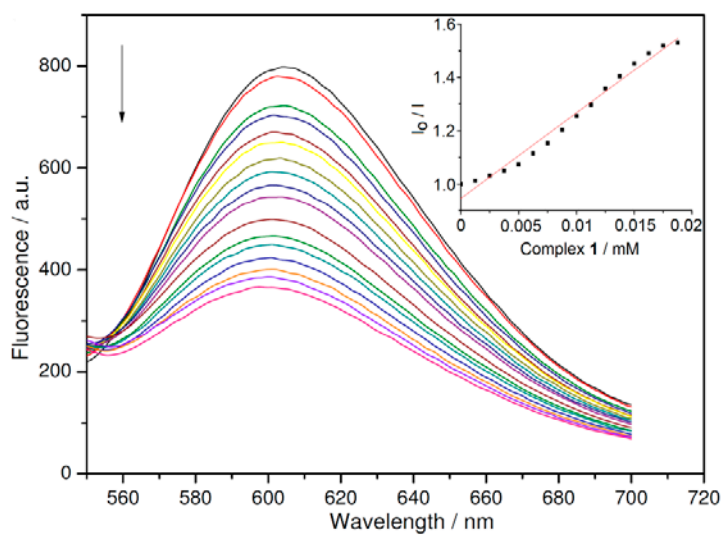


ACCEPTED

MANUSCRIPT

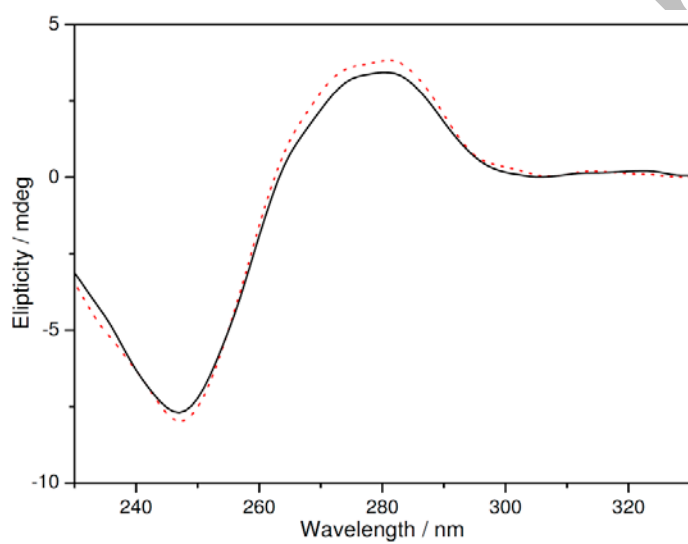
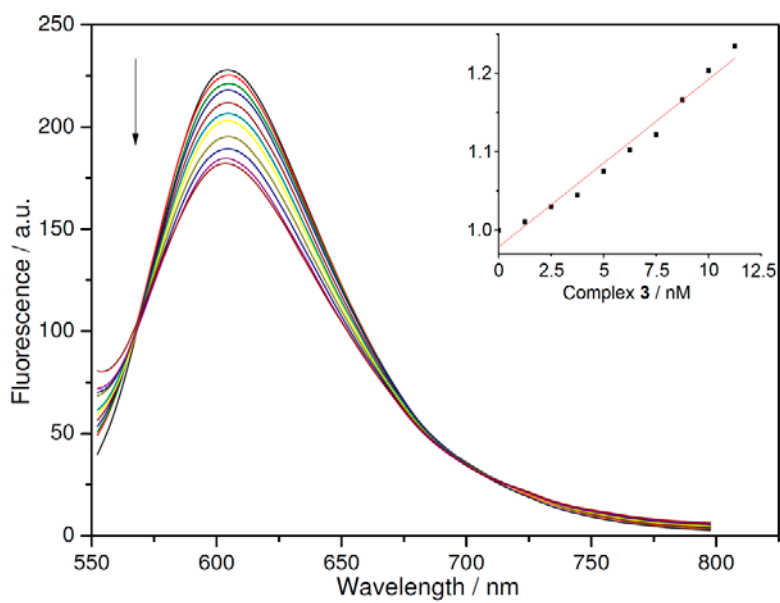


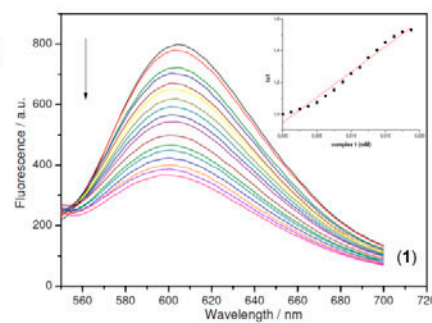
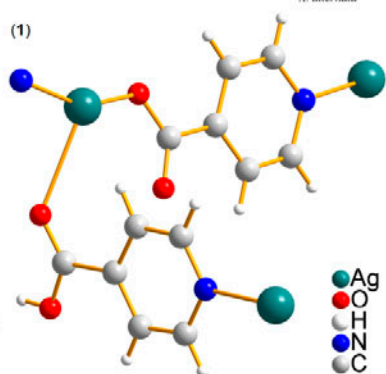
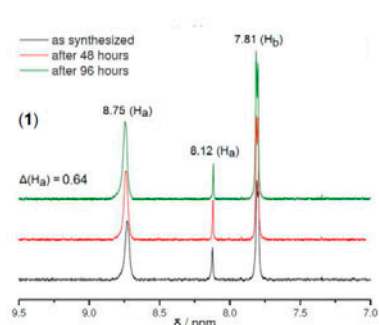
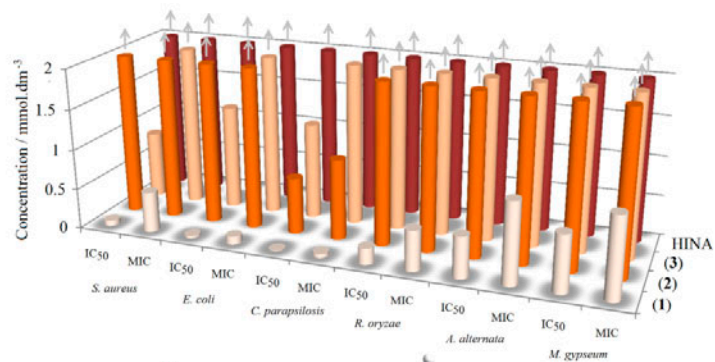
AC



Accepted

Manuscript





Accepted Manuscript

Table 1. Crystal data and structure refinement for 1.

Empirical formula	$C_{24}H_{17}Ag_3N_4O_8$
Formula weight	813.03
Temperature	173(2) K
Wavelength	0.71073 Å
Crystal system	Monoclinic
Space group	$P 2_1/c$
Unit cell dimensions	$a = 8.1779(4)$ Å $\alpha = 90^\circ$ $b = 19.5901(14)$ Å $\beta = 92.807(5)^\circ$ $c = 7.4107(5)$ Å $\gamma = 90^\circ$
Volume	$1\,185.96(12)$ Å ³
Z	2
Density (calculated)	2.280 g.cm ⁻³
Absorption coefficient	2.514 mm ⁻¹
$F(000)$	788
Crystal size	$0.2011 \times 0.2000 \times 0.1397$ mm ³
Theta range for data collection	3.247 to 26.494°
Index ranges	$-10 \leq h \leq 10$; $-24 \leq k \leq 23$; $-9 \leq l \leq 9$
Reflections collected	12 653
Independent reflections	2 459 [$R(\text{int}) = 0.0285$]
Completeness to theta (26.50°)	99.8 %
Absorption correction	Numerical
Max. and min. transmission	0.58 and 0.43
Refinement method	Full-matrix least-squares on F^2
Data / restraints / parameters	2 459 / 0 / 179
Goodness-of-fit on F^2	1.235
Final R indices [$I > 2\sigma(I)$]	$R_1 = 0.0278$, $wR_2 = 0.0804$
R indices (all data)	$R_1 = 0.0359$, $wR_2 = 0.0944$
Largest diff. peak and hole	0.732 and -1.356 e.Å ⁻³

Table 2. Selected bond distances (Å) and angles (°) for **1**.

Bond distances			
Ag(2)–N(2)#2	2.148(3)	O(3)–C(7)	1.218(4)
Ag(2)–N(2)	2.147(3)	O(4)–C(7)	1.279(4)
Ag(1)–O(1)	2.132(3)	O(1)–C(1)	1.268(4)
Ag(1)–O(3)	2.660(2)	O(2)–C(1)	1.231(4)
Ag(1)–N(1)#1	2.170(3)	O(4)–H(1O4)	0.8400
Bond angles			
O(3)–Ag(1)–O(1)	113.96(9)	C(4)–N(1)–Ag(1)#3	120.1(2)
O(3)–Ag(1)–N(1)#1	87.81(9)	C(10)–N(2)–Ag(2)	123.1(2)
O(1)–Ag(1)–N(1)#1	155.8(1)	C(11)–N(2)–Ag(2)	119.4(2)
N(2)–Ag(2)–N(2)#2	180.0(1)	O(2)–C(1)–O(1)	125.8(3)
C(7)–O(3)–Ag(1)	132.3(2)	O(3)–C(7)–O(4)	125.5(3)
C(1)–O(1)–Ag(1)	115.8(2)	C(7)–O(4)–H(1O4)	109.5(3)
C(5)–N(1)–Ag(1)#3	122.5(2)		

Symmetry transformations used to generate equivalent atoms: #1 $x-1, -y+3/2, -z+1/2$; #2 $-x+1, -y+1, -z+2$; #3 $x+1, -y+3/2, z-1/2$

Table 3. Possible hydrogen bonds (Å, °) for **1**.

D–H...A	d(D–H)	d(H...A)	d(D...A)	<(DHA)
C(4)–H(4)...O(3)#3	0.95	2.37	3.126(4)	136.3
C(10)–H(10)...O(2)#4	0.95	2.62	3.386(4)	138.1
C(11)–H(11)...O(2)#5	0.95	2.46	3.268(4)	142.9
C(4)–H(4)...O(3)#3	0.95	2.37	3.126(4)	136.3
C(10)–H(10)...O(2)#4	0.95	2.62	3.386(4)	138.1
C(11)–H(11)...O(2)#5	0.95	2.46	3.268(4)	142.9

Symmetry transformations used to generate equivalent atoms: #1 $x-1, -y+3/2, z+1/2$; #2 $-x+1, -y+1, -z+2$; #3 $x+1, -y+3/2, z-1/2$; #4 $x, y, z+1$; #5 $-x+1, -y+1, -z+1$

Table 4. The IR spectral data assignments for *catena*-[[Ag₃(INA)₃(HINA)]]_n (**1**), *catena*-[[Zn₂(INA)₄]_n (**2**), [Zn(INA)₂(H₂O)₄] (**3**), HINA and NaINA compounds (INA – isonicotinate) (band positions are in cm⁻¹).

	Compound				
	1	2	3	HINA	NaINA
$\nu(\text{OH})$	3411(m, br)		3411(m, br)	3380(m, br)	3450(w)
$\nu(\text{CH})_{\text{ar}}$	3107(w), 3039(w),		3096(w), 3050(w)	3122(w), 3103(w), 3086(w), 3072(w), 3053(w), 3008(w)	3070(vw)
$\nu(\text{NH}^+)_{\text{ar}}$	-			2260(w, br)	-
$\nu(\text{C}=\text{O})$	1715	-		1697(s, br)	-
$\nu(\text{C}=\text{C})_{\text{ar}}$ resp.	1608(vs)	1558(vs),	1562(vs),	1611(s),	1584(s)
$\nu(\text{C}=\text{N})_{\text{ar}}$	1392(vs)	1424(s),	1424(vs)	1563(w), 1409(w)	
$\nu_{\text{as}}(\text{COO}^-)$	1543(vs)	1614(vs)	1627(vs)	-	1534(s)
$\nu_{\text{s}}(\text{COO}^-)$	1347(vs)	1385(vs)	1365(s)	-	1410(s)
$\nu(\text{C}-\text{O})+\delta(\text{OH})$	1227(m)	1234(w)	1234(w)	1231(s)	1217(w)
$\delta(\text{CCH})$	1146(m), 1096(w), 1030(m)	1057(w), 1024(m)	1050(m), 1031(m)	1038(w), 1078(m)	1058(w)
$\beta(\text{CH})_{\text{ar}}$				1025(m)	1005(vw)
$\gamma(\text{OH})$				-	-
$\beta(\text{COO}^-)_{\text{s}}$				-	848(s)
$\delta(\text{COO}^-)$	690(vs)	690(s)	693(s)	-	679(s)
$\gamma(\text{CCH})_{\text{ar}}$	770(vs),	775(s)	775(s)	756(s), 698(vs)	764(s), 707(s)
$\beta(\text{COO})_{\text{as}}$				-	574(br)
$\gamma(\text{CCC})_{\text{ar}}$				477(w)	430(m)
δ_{r}	0.033 0.061	0.057	0.001	-	-
$\theta_{\text{OCO}-120}$	5.937 5.295	5.933	5.955	-	-
$\Delta_{\text{clcd.}}$	224, 268	268	167	-	-
$\Delta(\nu_{\text{as}}-\nu_{\text{s}})_{\text{IR}}$	196	230	262	-	124

vw – very weak, w – weak, m – medium, s – strong, vs – very strong, br – broad

Table 5. Antimicrobial activity of silver(I) and zinc(II) nitrates, free isonicotic acid and its silver(I) and zinc(II) complexes.

	Bacteria				Yeasts				Filamentous fungi			
	<i>S. aureus</i>		<i>E. coli</i>		<i>C. parapsilosis</i>		<i>R. oryzae</i>		<i>A. alternata</i>		<i>M.gypseum</i>	
	IC ₅₀	MIC	IC ₅₀	MIC	IC ₅₀	MIC	IC ₅₀	MI C	IC ₅₀	MI C	IC ₅₀	MIC
HINA	>2	>2	>2	>2	>2	>2	>2	>2	>2	>2	>2	>2
AgNO ₃	0.01	0.05 s	0.00 2	0.005 s	0.00 1	0.005 s	0.05 3	0.1 s	0.06 6	0.1 s	0.08	0.5s
Zn(NO ₃) ₂ ·6H ₂ O	0.5	>2	1.35	>2	0.24	2s	1.2	2s	1	2s	1	2s
Complex 1	0.06 8	0.5c	0.03	0.1s	0.00 7	0.05s	0.20	0.5 s	0.51	1c	0.70	1s
Complex 2	>2	>2	>2	>2	0.70	1s	>2	>2	>2	>2	>2	>2
Complex 3	0.84	>2	1.3	>2	1.2	2s	>2	>2	>2	>2	>2	>2

s – microbistatistical effect, c – microbicidal effect

Accepted Manuscript

Table 6. Electronic absorption data of **1-3**.

Compound	λ_{\max} [nm]		$\Delta\lambda$ [nm]	Hypochromism [%]
	Free	Bound		
1	216	217	1	2.24
	267	269	2	50.11
2	212	215	3	3.46
	267	268	1	8.13
3	211	212	1	2.31
	266	268	2	26.97

Accepted Manuscript